Construction and Building Materials 505 (2025) 144798

Contents lists available at ScienceDirect

Construction and Building Materials

journal homepage: www.elsevier.com/locate/conbuildmat

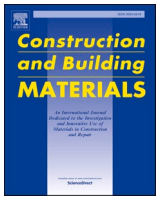

A dynamic approach to grading fast-grown Chinese fir: Correlating resonance frequency-derived modulus with mechanical properties

Fanxu Kong [a], Jingkang Lin [b], Yihe Ni [a], Jiangbo Du [c], Baolei Jin [a], Chenyang Jin [a], Shuke Jia [a], Zeli Que [a,*], Jianzhang Li [d]

[a] College of Material Science and Engineering, Nanjing Forestry University, Nanjing, Jiangsu 210037, China
[b] Fujian Provincial Institute of Architectural Design and Research Co., Ltd., Fuzhou 350001, China
[c] Jiangsu Desong Wood Industry Co., Ltd., Zhangjiagang, Jiangsu 215600, China
[d] State Key Laboratory of Efficient Production of Forest Resources, Beijing Forestry University, Beijing 100083, China

ARTICLE INFO

Keywords:
Fast-grown Chinese fir
Resonance frequency method
Dynamic modulus of elasticity
Monte Carlo simulation
Mechanical grading

ABSTRACT :

In response to carbon neutrality goals and policies promoting sustainable construction, timber structures are receiving increasing attention in China. However, the structural timber market still relies heavily on imports, while fast-grown domestic plantation species such as Chinese fir (*Cunninghamia lanceolata* (Lamb.) Hook) remain underutilized for structural applications due to the lack of reliable grading systems. This study investigated the grading potential of fast-grown Chinese fir using non-destructive evaluation. A total of 162 laminae with varying dimensions were tested. The dynamic modulus of elasticity (MOE) was determined using the resonance frequency method, and regression models were developed to predict static bending MOE and bending strength. The results of the goodness-of-fit and model comparison, based on the one-sample Kolmogorov–Smirnov (K-S) test and the Akaike Information Criterion (AIC), indicated that the density, dynamic MOE, bending MOE, and bending strength all more closely follow a lognormal distribution. Monte Carlo simulations were performed to assess the influence of specimen dimensions on resonance frequencies, showing maximum absolute mean prediction errors of 2.31 % and 4.52 % for longitudinal and transverse frequencies, respectively. Threshold values of dynamic MOE corresponding to the strength classes defined in Japanese standard JAS 1152 were derived using the prediction limit method. The laminae were classified into six grades (including a Reject grade), with dynamic MOE thresholds ranging from 5.4 to 6.9 GPa, primarily determined by the lower limit of bending MOE. Most specimens (47.5 %) fell into grade L40, a strength class which requires a minimum average bending MOE of 4.0 GPa (lower limit 3.3 GPa) and a minimum average bending strength of 24.0 MPa (lower limit 18.0 MPa). All assigned grades satisfied the JAS 1152 requirements for mean and lower limit of bending MOE and strength, except grade L60 (another JAS 1152 strength class), which exhibited a slightly lower bending MOE (4.2 GPa) than the 5.0 GPa standard lower limit. The findings provide a technical basis for strength grading of fast-grown Chinese fir, supporting its structural utilization and contributing to reduced dependence on imported timber in modern Chinese timber construction.

1. Introduction

Amid the global pursuit of carbon neutrality, China has been actively promoting timber construction as a sustainable alternative to traditional concrete and steel systems. Modern engineered wood products—such as glued laminated timber (glulam) and cross-laminated timber (CLT)—play a crucial role in this transition due to their low embodied carbon, favorable strength-to-weight ratio, and renewability [1–3]. However, the structural timber used in these products still relies predominantly on imports. Commercial species such as spruce (*Picea* spp.), pine (*Pinus* spp.), fir (*Abies* spp.), and Douglas fir (*Pseudotsuga menziesii*), which are widely used in glulam and CLT production, are generally strength-graded before export [4]. This reliance on imported materials presents challenges regarding cost control, supply chain stability, and long-term sustainability [1,5,6].

In contrast, China possesses the world's largest plantation forest

* Corresponding author.
E-mail address: zelique@njfu.edu.cn (Z. Que).

https://doi.org/10.1016/j.conbuildmat.2025.144798
Received 7 August 2025; Received in revised form 21 October 2025; Accepted 5 December 2025
Available online 8 December 2025

area, with Chinese fir (*Cunninghamia lanceolata* (Lamb.) Hook) as one of the most widely cultivated fast-growing softwoods. This species is characterized by its rapid growth, high yield, and natural durability, making it a promising candidate for structural applications [7,8]. Despite these attributes, Chinese fir is mainly processed into low-value-added products such as particleboard, plywood, and pulp [9,10]. Historically, Chinese fir has been a core material in traditional timber architecture. Even today, in villages or regions within provinces such as Guizhou, Fujian, Yunnan, etc., it continues to be used in mortise-and-tenon wood dwellings for load-bearing components including beams, columns, and purlins [11]. However, its utilization remains largely limited to roundwood and sawn lumber, which exhibit substantial variability in material properties. At present, structural performance is often ensured by empirically increasing cross-sectional dimensions. Developing effective grading, finger-jointing, and lamination techniques for engineered structural components could significantly reduce strength variability [6]. Nevertheless, a key barrier to its broader adoption in modern timber structural applications is the lack of a standardized grading system specifically designed for domestic fast-grown species.

Over the past decades, both domestic and international efforts have focused on developing mechanical grading approaches for fast-grown timbers, with increasing attention to non-destructive testing (NDT) methods [12,13]. Among these, resonance-based techniques have proven especially effective in estimating the dynamic modulus of elasticity (MOE), which serves as a strong and reliable predictor for mechanical performance [14]. For example, Arriaga et al. demonstrated that both longitudinal and transverse vibration methods produced strong correlations with static MOE for Radiata pine (*Pinus radiata*) (R^2 = 0.87 and 0.86, respectively), with the longitudinal method being more suitable for industrial use due to its simpler operation and lower slenderness requirements [12]. Similarly, França et al. reported robust correlations (R^2 = 0.85–0.89) between dynamic and static MOE in Southern pines (*Pinus* spp.) across multiple vibration devices, although the correlation between dynamic MOE and bending strength was weaker (R^2 = 0.38–0.45) [15]. Studies on fast-growing *Eucalyptus grandis* by Ettelaei et al. further confirmed the reliability of acoustic NDT methods, reporting a strong correlation (R^2 = 0.89) between dynamic MOE obtained from wave velocity and static MOE [16]. Balasso et al. also observed that the correlation between dynamic MOE in the green state (moisture content >25 %) and final static MOE improved significantly after drying and planing (R^2 increased from 0.59 to 0.69), highlighting the potential for early-stage stiffness screening during processing [17].

In China, similar studies have examined Chinese fir for structural use. Ou et al. established dynamic grading intervals based on for Chinese fir laminae used in glulam, demonstrating reduced variability in bending performance and significant influence of both lamina grade and lay-up configuration on final product performance [18]. Gong et al. evaluated glulam fabricated from Chinese fir and reported that products composed of both uniform and mixed-grade laminae met the strength (≥28 MPa or ≥24 MPa) and stiffness (MOE ≥8000 MPa) requirements specified for TC_T28 and $TC_{YD}24$ grades in GB/T 26899 [6,19]. These studies collectively confirmed the feasibility of manufacturing glulam from Chinese fir. They also highlighted that grading based on dynamic MOE and optimizing lamina lay-up can effectively enhance the mechanical performance of glulam. Additional research has also explored the application of Chinese fir in CLT panels [8,20].

Despite these advances, several critical issues remain to be addressed:

- For Chinese fir, fundamental data on resonance frequencies across varying dimensions are limited. In particular, the dimensional dependence of longitudinal and transverse fundamental frequencies—critical for estimating dynamic MOE—remains unclear.
- In previous studies on Chinese fir, grading intervals were often determined solely using dynamic MOE and applied in glulam lay-up design, without direct validation against code-defined static strength grades.
- While China's glulam standard GB/T 26899 [19]—adapted from Japan's JAS 1152 [21]—requires flatwise static bending tests for lamina grading, most experimental studies on fast-grown plantation species have employed edgewise bending tests.

These discrepancies highlight the need for a harmonized and data-supported grading framework that reflect both domestic resource characteristics and standardization requirements.

To address these challenges, this study investigates the feasibility of using resonance frequency methods to determine the dynamic MOE of fast-grown Chinese fir and evaluates its potential for mechanical grading. It further analyzes the statistical characteristics and dimensional effects of resonance-derived dynamic MOE and density to ensure the reliability of dynamic measurements across varying specimen sizes. Quantitative relationships between dynamic and static bending properties are established through regression modeling, providing a predictive basis for mechanical grading. Finally, the study assesses the grading thresholds of dynamic MOE corresponding to the strength classes defined in JAS 1152 [21], supporting the development of a resonance-based grading framework tailored to domestic fast-grown timber. Collectively, these objectives aim to provide a scientific foundation for the structural utilization of Chinese fir, promoting its high-value application and contributing to the reduction of dependence on imported structural timber in China's sustainable construction sector.

2. Material and methods

2.1. Material and specimens

Chinese fir timber was sourced from Nanping City, Fujian Province, China, with tree ages of 10–13 years. A total of 162 specimens were prepared based on a full factorial combination of three levels of thickness (13, 18, and 35 mm), width (45, 60, and 90 mm), and length (750, 1500, and 3000 mm), with six replicates per combination. The average moisture content was 13.04 % (standard deviation 2.47 %). Density and mechanical properties are detailed in subsequent sections.

Only visually sound pieces without decay or discoloration were selected; minor surface cracks were permitted if no wider than 0.5 mm and no longer than 15 mm. Unlike Machine Stress Rating (MSR) systems, grading based on the resonance frequency method evaluates the dynamic MOE along the full length of the member. In accordance with the provisions of JAS 1152 [21], no restrictions were imposed on knots or holes in this study, as their effects on the global stiffness were inherently captured in the resonance measurement.

2.2. Moisture content and density measurements

Moisture content was measured after bending tests by extracting a small specimen near the failure zone, with a longitudinal length of at least 20 mm, using the oven-dry method.

Density was determined following the method in [12]. During non-destructive testing, global density (ρ_{global}) was calculated as mass divided by volume. In bending tests, local density (ρ_{local}) was measured using a full cross-section specimen (20 mm long) taken near the failure area. Mass and volume of the same specimen were recorded, and it was also used for moisture content determination.

Following [14], local density was adjusted to 12 % moisture content ($\rho_{local,12}$) based on the measured moisture content (u) using Eq. (1). Global density was similarly adjusted to 12 % moisture content ($\rho_{global,12}$) using Eq. (2), with the average moisture content (u_s) of all specimens.

$$\rho_{local,12} = \rho_{local}(1 - 0.005(u - 12)) \quad (1)$$

$$\rho_{global,12} = \rho_{global}(1 - 0.005(u_s - 12)) \quad (2)$$

2.3. Dynamic MOE tests

In this study, dynamic MOE was measured using a resonance frequency testing device (Model IET-5, manufactured in Henan, China), with a frequency response range of 20 Hz to 22 kHz and a resolution of 0.1 Hz. The longitudinal and transverse dynamic MOE were calculated using Eq. (3) and Eq. (4) respectively, and adjusted to 12 % moisture content following [12,14].

$$E_{dyn,l,12} = 4\frac{m}{L \bullet h \bullet b} \bullet f^2 \bullet L^2 \left(1 + \frac{u_s - 12}{100}\right) \times 10^{-9} \quad (3)$$

Where $E_{dyn,l,12}$ is the longitudinal dynamic MOE (GPa), f is the first longitudinal frequency (Hz), m is the mass (kg), L, h and b are the specimen's length, thickness, and width (m).

$$E_{dyn,t,12} = \left(\frac{2f_1}{\gamma_1 \bullet \pi}\right)^2 \bullet \frac{m \bullet L^3}{I} \left(1 + \frac{u_s - 12}{100}\right) \times 10^{-9} \quad (4)$$

Where $E_{dyn,t,12}$ is the transverse dynamic MOE (GPa), f_1 is the first transverse frequency (Hz), $\gamma_1 = 2.267$, and I is the cross-sectional moment of inertia (m^4).

Eq. (3) is derived from the classical solution for the fundamental longitudinal vibration of a prismatic bar under free-free boundary conditions. The expression for the dynamic MOE in the longitudinal fundamental mode is:

$$E_{dyn,l} = \rho(2fL)^2 \quad (5)$$

By substituting the density ρ, which equals ρ_{global} in Eq. (2) with $m/(L \bullet h \bullet b)$, and noting that f represents the resonance frequency of the first longitudinal mode, Eq. (6) is obtained.

$$E_{dyn,l} = 4\frac{m}{L \bullet h \bullet b} \bullet f^2 \bullet L^2 \quad (6)$$

A moisture content adjustment term, $\left(1 + \frac{u_s - 12}{100}\right)$, is incorporated based on wood mechanics conventions and the reference [14], and a factor of 10^{-9} is applied to convert the result into GPa, yielding the final form of Eq. (3).

Eq. (4) is based on Euler-Bernoulli beam theory for a free-free beam vibrating in its first flexural mode. The general form of the dynamic MOE in transverse vibration is:

$$E_{dyn,t} = \left(\frac{2\pi f_1}{{\beta_1}^2}\right)^2 \bullet \frac{mL^3}{I} \quad (7)$$

Where f_1 is the first transverse resonance frequency, β_1 is the dimensionless frequency parameter for the first mode. For a free-free beam, $\beta_1 = 4.7300408$. Letting $\gamma_1 = {\beta_1}^2/\pi^2 \approx 2.267$, the expression simplifies to the form used in Eq. (4), and the same moisture content adjustment and unit conversion as in Eq. (3) are applied.

As shown in Fig. 1, both frequencies (f and f_1) were extracted from vibration signals using Fourier Transform. In the longitudinal dynamic MOE test (Fig. 1-a), the specimen was simply supported on polyurethane foam pads. A hammer struck one end to induce vibration, and a microphone at the opposite end captured the signal. For transverse dynamic MOE testing (Fig. 1-b), supports were placed at nodal points (0.224 L from each end). The specimen was struck at mid-span, and a microphone positioned near and above the end recorded the response. These frequencies, along with specimen mass and dimensions, were used to compute the dynamic MOE in both directions.

2.4. Static bending tests

Static bending tests were conducted using an electronic universal testing machine (model UTM5105, maximum capacity 100 kN) manufactured by Shenzhen Sansi Zongheng Technology Co., Ltd. Before testing, each specimen was visually inspected along its entire length to identify potential strength-reducing features, including the largest knot or hole, pronounced grain deviation, and visible cracks. The method for measuring these defects followed the Japanese standard JAS 1083 [22]. The cross-section containing the most critical defect or combination of defects, which was considered most likely to govern bending failure, was assumed to represent the weakest section. In the experimental setup, this section was positioned directly under the loading head in three-point bending, and midway between the two loading heads in four-point

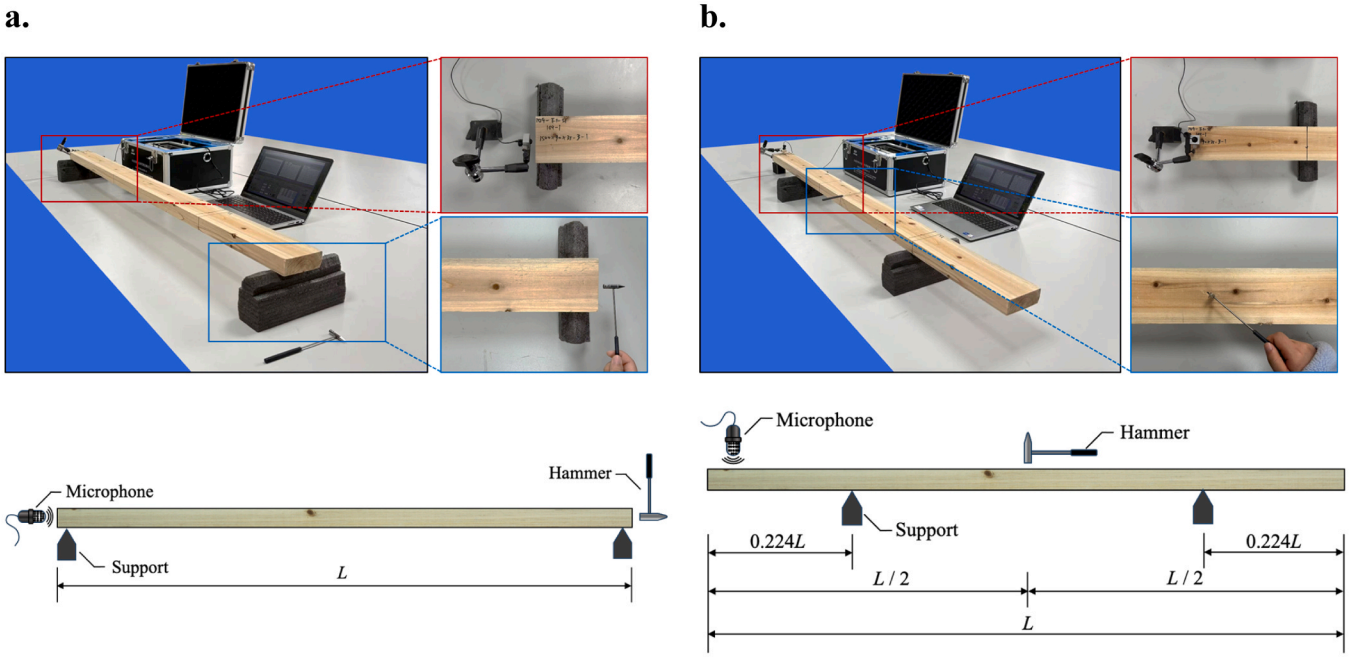

Fig. 1. Experimental setup and schematic diagram for dynamic MOE testing: (a) longitudinal dynamic MOE; (b) transverse dynamic MOE.

bending.

The bending MOE was determined using a three-point bending test (Test B) in accordance with JAS 1152 [21], as shown in Fig. 2-a. Specifically, the maximum applied load was set as the upper limit of the elastic range, and deflection was measured using a linear variable differential transformer (LVDT) as the difference in displacement under two load levels. The lower and upper limits of the elastic range were defined to 10 % and 40 % of the estimated maximum failure load, respectively, and bending MOE was calculated accordingly.

The estimated failure load was obtained by testing ten specimens randomly cut from areas outside the regions used for the bending MOE tests of 3000 mm specimens. The mean of these measured maximum loads was taken as the estimated failure load for each cross-section. Table 1 summarizes the average maximum load, standard deviation, and coefficient of variation for all cross-sectional sizes.

According to JAS 1152 [21], the loading rate was maintained below 14.7 MPa/min, and in this study, it was controlled at approximately 13.0 MPa/min. The stress rate ($\dot{\sigma}$) was converted to the corresponding loading rate ($\dot{P}$) using Eq. (8), where l is the span. Table 1 also shows the corresponding loading rates for each cross-sectional size.

$$\dot{P} = \frac{2bh^2}{3l} \times \dot{\sigma} \tag{8}$$

Each test was terminated when the applied load reached the upper limit of the elastic range, and bending MOE at 12 % moisture content was calculated using Eq. (9):

$$E = \frac{\Delta P l^3}{4bh^3 \Delta y}(1 + 0.015(u - 12)) \bullet 10^{-3} \tag{9}$$

where E is the bending MOE (GPa), ΔP is the load difference (N), and Δy is the corresponding mid-span deflection under ΔP (mm).

Bending strength was determined using a four-point bending test (Test C) per JAS 1152 [21], as shown in Fig. 2-b. The loading rate was also maintained below 14.7 MPa/min and controlled at 13.0 MPa/min during testing. Unlike the procedure described for the three-point bending test, under four-point bending conditions, the stress rate ($\dot{\sigma}$) was converted to the corresponding load rate ($\dot{P}$) using Eq. (10):

$$\dot{P} = \frac{bh^2}{l} \times \dot{\sigma} \tag{10}$$

The calculated load rates for the nine cross-sectional sizes are also summarized in Table 1.

Each test was terminated when visible damage occurred or when the applied load decreased to less than 80 % of the maximum recorded load, and bending Strength at 12 % moisture content was calculated using Eq. (11):

$$f = \frac{Pl}{bh^2}(1 + 0.04(u - 12)) \tag{11}$$

where f is bending strength (MPa), P is max load (N).

It should also be noted that although the 750 mm-long and 35 mm-thick specimens met the minimum required span-to-depth ratio of 21, the supports were positioned too close to the specimen ends, leaving only 7.5 mm on each side. Therefore, the tests were conducted using a reduced span equivalent to 20 times the thickness.

2.5. Grading procedure for laminae

2.5.1. Strength class requirements

According to JAS 1152 [21], the average bending MOE for mechanically graded lamina specimens must meet the specified grade mean and all individuals must not fall below the grade lower limit. Moreover, the standard specifies different requirements for laminae depending on their position in the glulam and the product type. Specifically:

- For symmetric heterogeneous glulam: laminae used as the outermost and outer layers.
- For asymmetric heterogeneous glulam: laminae used as the outermost and outer layers on the tension side.
- For glulam composed of uniform grades: all laminae used in the product.

For these laminae, the following requirements apply:

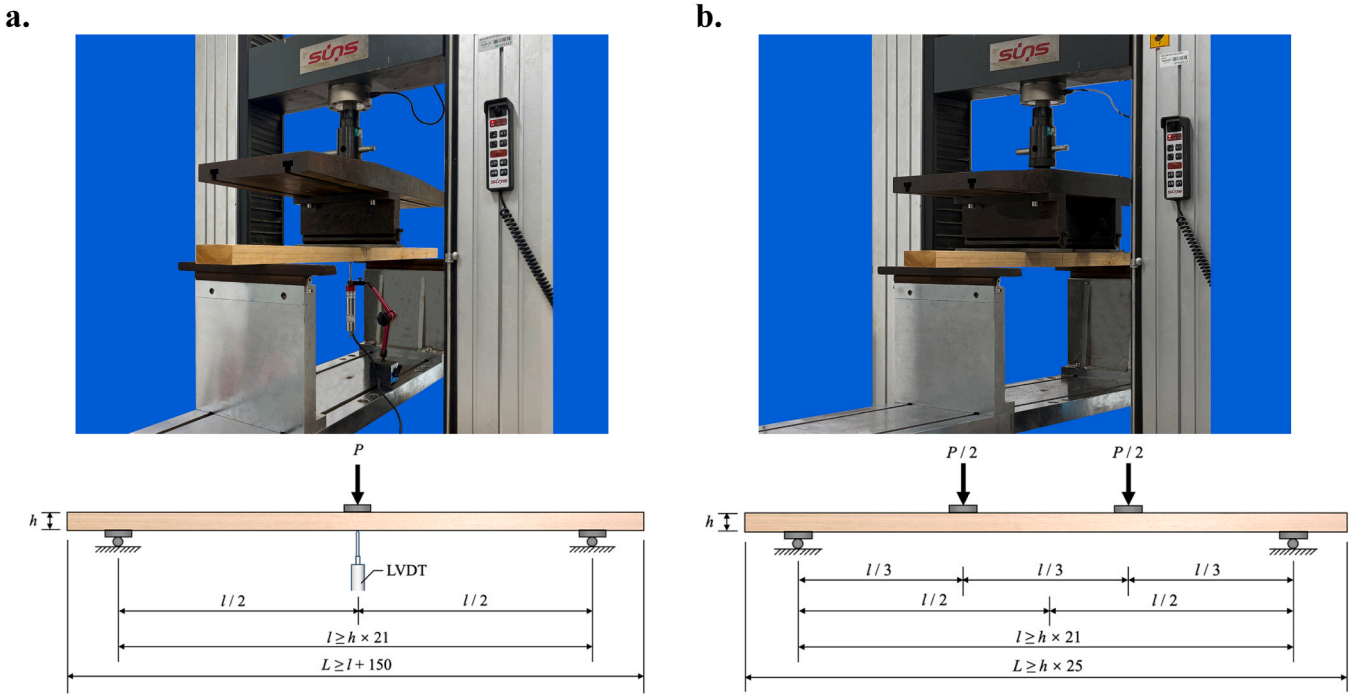

Fig. 2. Setup and schematic diagrams of the bending tests: (a) bending MOE; (b) bending strength.

Table 1
Failure load statistics and derived loading parameters for bending tests.

Specimen design parameters				Statistics of failure loads			Elastic Range (N)		Rate of loading (N/min)	
Thickness (mm)	Width (mm)	Span (mm)	Replicates	Mean (N)	Sd (N)	Cv (%)	Lower limit	Upper limit	3-point bending	4-point bending
13	45	273	10	1239	264	21.27	124	496	241	362
	60			1342	342	25.50	134	537	322	483
	90			2140	389	18.16	214	856	483	724
18	45	378		1587	200	12.62	159	635	334	501
	60			1846	251	13.58	185	738	446	669
	90			3083	430	13.83	308	1233	669	1003
35	45	735		2495	449	18.00	250	998	650	975
	60			3588	646	18.02	359	1435	867	1300
	90			4785	924	19.31	479	1914	1300	1950

Note: For specimens with a length of 750 mm and a thickness of 35 mm, the span was set to 700 mm (20 times the thickness). For specimens with widths of 45, 60, and 90 mm, the loading rates in the three-point bending test were 683, 910, and 1365 N/min, respectively, while those in the four-point bending test were 1024, 1365, and 2048 N/min, respectively.

- Based on three-point bending tests (Fig. 2-a), the mean MOE must meet or exceed the specified grade mean, and at least 95 % of specimens must meet the grade's lower limit.
- For longitudinal finger-jointed laminae, tested in bending as shown in Fig. 2-b, the mean bending strength must meet or exceed the specified grade mean, and 95 % of specimens must reach the lower strength limit.

To evaluate the proposed mechanical grading method, this study designed experiments consistent with JAS 1152 [21]:

- Lamina specimens (although non-finger-jointed) were tested for bending MOE and bending strength to meet the requirements for various glulam configurations.
- Grading was benchmarked against JAS 1152 [21] grade levels (e.g., L30, L40, L50), requiring compliance with both mean property targets and 95 % lower limits at 75 % confidence level. For instance, L50-grade lamina must exhibit an average bending MOE $\geq$ 5.0 GPa (lower limit: 4.1 GPa) and average bending strength $\geq$ 27.0 MPa (lower limit: 20.5 MPa).

2.5.2. Derivation of mechanical grading settings

To establish mechanical grading settings, regression models correlating the measured dynamic MOE with the static bending MOE and bending strength were developed. As JAS 1152 [21] does not prescribe a method for deriving grading settings, this study refers to the prediction limit method recommended in EN 14081–2 [23]. Using this approach, the dynamic MOE thresholds corresponding to the required mean and lower-limit values of bending MOE and bending strength were calculated using Eq. (12) – Eq. (16):

$$S_{E,\mathrm{mean}} = \frac{E_{\mathrm{req,mean}} - b_E}{a_E} \tag{12}$$

$$S_{E,05} = \frac{E_{\mathrm{req},05} - b_E + t_{\alpha,n-2} \bullet s_{\delta,E}}{a_E} \tag{13}$$

$$S_{f,\mathrm{mean}} = \frac{f_{\mathrm{req,mean}} - b_f}{a_f} \tag{14}$$

$$S_{f,05} = \frac{f_{\mathrm{req},05} - b_f + t_{\alpha,n-2} \bullet s_{\delta f}}{a_f} \tag{15}$$

$$S = \mathrm{Max}\left\{S_{E,\mathrm{mean}}, S_{E,05}, S_{f,\mathrm{mean}}, S_{f,05}\right\} \tag{16}$$

Here, S is the grading threshold: if a specimen's dynamic MOE exceeds S, the corresponding bending MOE and strength are expected to meet the grade requirements ($E_{\mathrm{req,mean}}$, $E_{\mathrm{req},05}$, $f_{\mathrm{req,mean}}$, and $f_{\mathrm{req},05}$). Parameters a_E, b_E and a_f, b_f are slopes and intercepts of the respective regression models. The term $t_{\alpha,n-2}$ represents the critical value from the t-distribution, accounting for the desired confidence level (α) and degrees of freedom ($n - 2$); for a 5 % prediction level with assumed large samples, $t_{0.05,\infty} = 1.645$.

Standard errors of the estimate, $s_{\delta,E}$ and $s_{\delta,f}$, were computed using Eq. (17) [24]:

$$s_\delta = \sqrt{\frac{n}{n-2}\left(1 - \frac{s_{X,Y}{}^2}{s_X{}^2 s_Y{}^2}\right) s_Y{}^2} \tag{17}$$

Where X is dynamic MOE and Y is either bending MOE or strength, depending on the model. s_X, s_Y, and $s_{X,Y}$ are the standard deviations and covariance of the variables.

2.6. Statistical analysis

The measured density, dynamic MOE, bending MOE, and bending strength were fitted using normal, lognormal, and two-parameter Weibull distributions. Their probability density functions are shown in Eq. (18) – Eq. (20):

$$f(x;\mu,\sigma^2) = \frac{1}{\sqrt{2\pi\sigma^2}} e^{-\frac{(x-\mu)^2}{2\sigma^2}} \tag{18}$$

$$f(x;\mu,\sigma^2) = \frac{1}{x\sigma\sqrt{2\pi}} e^{-\frac{(\ln x-\mu)^2}{2\sigma^2}} \tag{19}$$

$$f(x;k,\lambda) = \frac{k}{\lambda}\left(\frac{x}{\lambda}\right)^{k-1} e^{-\left(\frac{x}{\lambda}\right)^k} \tag{20}$$

The parameters of the normal distribution (mean μ; standard deviation σ) were estimated using the method of moments, while those of the lognormal distribution were obtained by applying the same method to logarithmically transformed data. The Weibull distribution parameters (shape k; scale λ) were estimated using the maximum likelihood method.

The goodness-of-fit of the normal, lognormal, and Weibull distributions was evaluated using the one-sample Kolmogorov–Smirnov (K–S) test. The K-S test statistic, denoted as D_n, represents the maximum absolute difference between the empirical cumulative distribution function (ECDF) of the sample and the cumulative distribution function (CDF) of the theoretical distribution, as shown in Eq. (21).

$$D_n = \max|F_n(x) - F(x)| \tag{21}$$

Here, $F_n(x)$ is the ECDF for a sample of size n, which at any value x is simply the proportion of observations in the sample that are less than or equal to x, is formally defined as Eq. (22).

$$F_n(x) = \frac{1}{n}\sum_{i=1}^{n} I_{\{x_i \le x\}} \tag{22}$$

Where $I_{\{x_i \le x\}}$ is the indicator function that equals 1 if $x_i \le x$ and 0 otherwise.

$F(x)$ denotes the CDF of the hypothesized theoretical distribution, giving the probability that a random variable drawn from this distribution is less than or equal to x.

The p-value associated with the K–S test quantifies the probability of observing a test statistic as large as, or larger than, the calculated D_n, assuming the null hypothesis that the sample data follow the specified theoretical distribution is true. A p-value greater than the significance level ($\alpha = 0.05$) indicates insufficient evidence to reject the null hypothesis, implying that the theoretical distribution provides an adequate fit to the observed data [25–27].

The critical value of the K-S statistic at the 5 % significance level, $D_{n,0.05}$, was calculated using Eq. (23), where n denotes the sample size. It should be noted that $D_{n,0.05}$ and the p-value represent equivalent approaches for hypothesis testing. A distribution was regarded as an acceptable fit only when both of the following conditions were satisfied: (1) the calculated D_n was smaller than $D_{n,0.05}$, and (2) the corresponding p-value exceeded 0.05.

$$D_{n,0.05} = \frac{1.35810}{\sqrt{n}}, \quad n > 50 \tag{23}$$

To quantitatively compare the relative quality of the three statistical models, the Akaike Information Criterion (AIC) was also employed [28]. The AIC is calculated as Eq. (24).

$$\mathrm{AIC} = -2\ln(\mathscr{L}) + 2k \tag{24}$$

where $\mathscr{L}$ is the value of the model's likelihood function, k is the number of estimated parameters. The model with the lowest AIC value is preferred, as it represents the best trade-off between goodness-of-fit and model complexity.

All statistical computations, including the D_n, p-value, and AIC calculation, as well as parameter estimation and regression modeling, were performed using the R programming language [29].

3. Results and discussion

3.1. Nondestructive tests

3.1.1. Density

Fig. 3 presents histograms of global and local density with fitted normal, lognormal, and Weibull curves. Table 2 summarizes the results of goodness-of-fit and model comparison based on one-sample K-S test and AIC. For global density, both normal and lognormal distributions are acceptable ($D_n < D_{n,0.05}$, $p > 0.05$), with the lognormal distribution showing a better fit (AIC = 1674.80) than the normal distribution (AIC = 1689.00). For local density, all three distributions provide acceptable fits. Although EN 14358 assumes a normal distribution [30], the AIC results indicated that the lognormal distribution offered the best fit (AIC = 1613.14) in this study.

Fig. 4 shows the regression relationship between global and local density, with a coefficient of determination $R^2 = 0.5958$, indicating a moderate correlation. In industrial practice, global density is relatively easy to determine, as it can be calculated online by weighing the timber and measuring its dimensions [12]. This facilitates the indirect estimation of local density for strength quality control.

3.1.2. Dynamic MOE

Fig. 5 shows the histograms of longitudinal and transverse dynamic MOE, fitted with normal, lognormal, and Weibull distributions. Table 3 presents the results of goodness-of-fit and model comparison based on one-sample K-S test and AIC, indicating that both longitudinal and transverse dynamic MOE conform only to the lognormal distribution ($D_n < D_{n,0.05}$, $p > 0.05$), while the normal and Weibull distributions exhibit significant deviations ($D_n > D_{n,0.05}$, $p < 0.05$).

Given the lognormal fit, the expected value $E(X)$ and standard deviation $\sigma(X)$ of dynamic MOE were calculated using Eq. (25) and Eq. (26), based on the estimated parameters μ and σ (Table 3):

$$E(X) = e^{\mu + \frac{\sigma^2}{2}} \tag{25}$$

$$\sigma(X) = \sqrt{(e^{\sigma^2} - 1)e^{2\mu+\sigma^2}} \tag{26}$$

Table 4 summarizes the sample statistics and lognormal estimates, including the 5th and 95th percentiles at 75 % confidence. The sample mean of longitudinal dynamic MOE (7.5023 GPa) closely matches the lognormal expected value (7.5017 GPa), indicating the sample mean is a reliable estimator, and a similar agreement is also observed in the transverse direction. This supports EN 14358, which allows using the sample mean for stiffness without requiring a distributional assumption [30].

Fig. 6 illustrates the regression between longitudinal and transverse dynamic MOE, revealing a strong correlation ($R^2 = 0.8963$). This confirms the scientific validity of both measurements for Chinese fir material across various specimen dimensions, based on the first resonance frequency. Notably, for 3-meter specimens, the transverse resonance frequency fell below the device's detection range (20 Hz to 22 kHz) and could not be measured. The analysis is therefore based on 108 specimens of shorter lengths. The following section details the theoretical

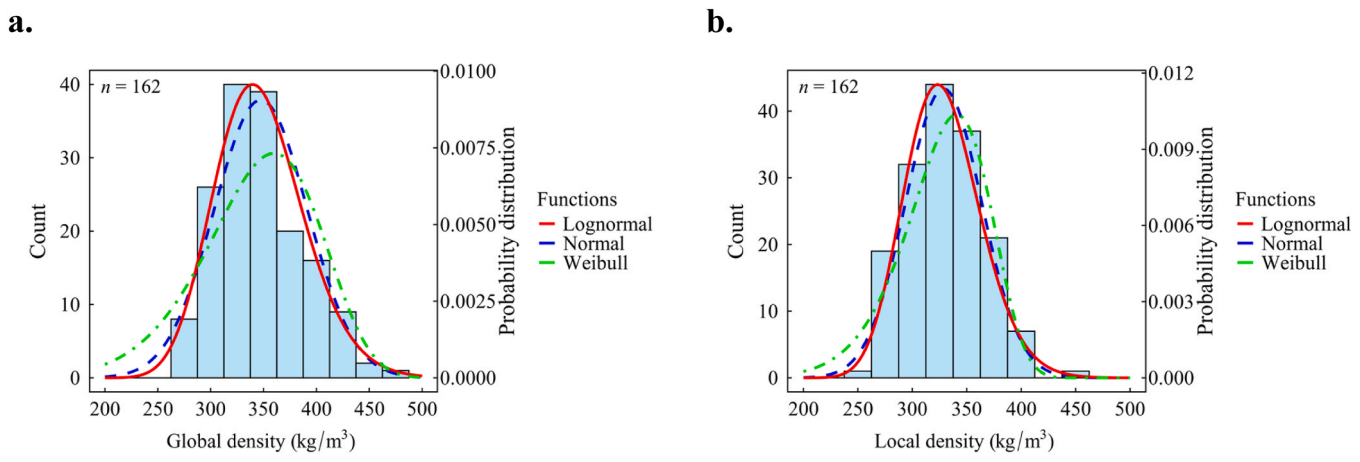

Fig. 3. Histograms of global (a) and local (b) density with fitted probability distributions.

Table 2
Goodness-of-fit and model comparison based on one-sample K-S test and AIC for global and local density.

Density type	Hypothetical distribution	Parameters					Judgement	AIC
Global density	Normal distribution	μ	σ	D_n	$D_{n,0.05}$	p-value		
		347.3806	43.8890	0.0843	0.1067	0.1995	accept	1689.00
	Lognormal distribution	5.8428	0.1218	0.0586	0.1067	0.6334	accept	1674.80
	Weibull distribution	k	λ	D_n	$D_{n,0.05}$	p-value		
		7.2364	367.2944	0.1241	0.1067	0.0137	refuse	1728.56
Local density	Normal distribution	μ	σ	D_n	$D_{n,0.05}$	p-value		
		328.7766	34.9363	0.0347	0.1067	0.9897	accept	1615.08
	Lognormal distribution	5.7897	0.1062	0.0511	0.1067	0.7911	accept	1613.14
	Weibull distribution	k	λ	D_n	$D_{n,0.05}$	p-value		
		9.6614	344.6835	0.0701	0.1067	0.4032	accept	1634.54

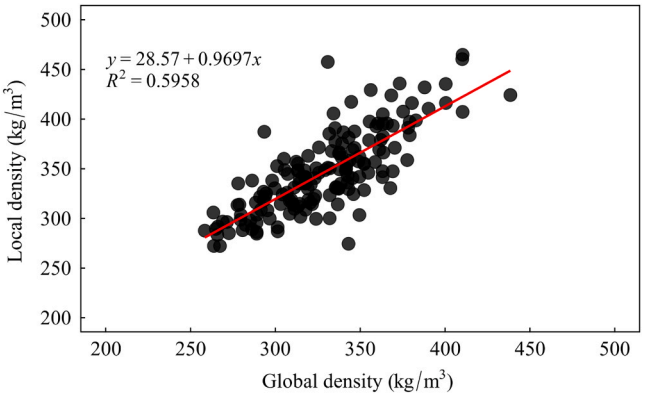

Fig. 4. Regression relationship between global and local density.

calculation of first resonance frequencies across different specimen dimensions.

3.1.3. Theoretical calculation for resonance frequencies

3.1.3.1. Longitudinal resonance frequency. The first longitudinal resonance frequency of each specimen can be theoretically determined by combining Eq. (2) and Eq. (3), which yielding Eq. (27).

$$E_{dyn,l,12} = 4\rho_{12} f^2 L^2 \frac{1 + 0.01(u_s - 12)}{1 - 0.005(u_s - 12)} \times 10^{-9} \tag{27}$$

Where ρ_{12} denotes $\rho_{global,12}$ as defined previously.

Given that the average moisture content was 13.04 %, substituting $u_s = 13.04$ simplifies Eq. (27) to Eq. (28).

$$f = \sqrt{\frac{E_{dyn,l,12}}{4.062728 \times 10^{-9} \bullet \rho_{12} L^2}} \tag{28}$$

Eq. (28) establishes the deterministic physical relationship between

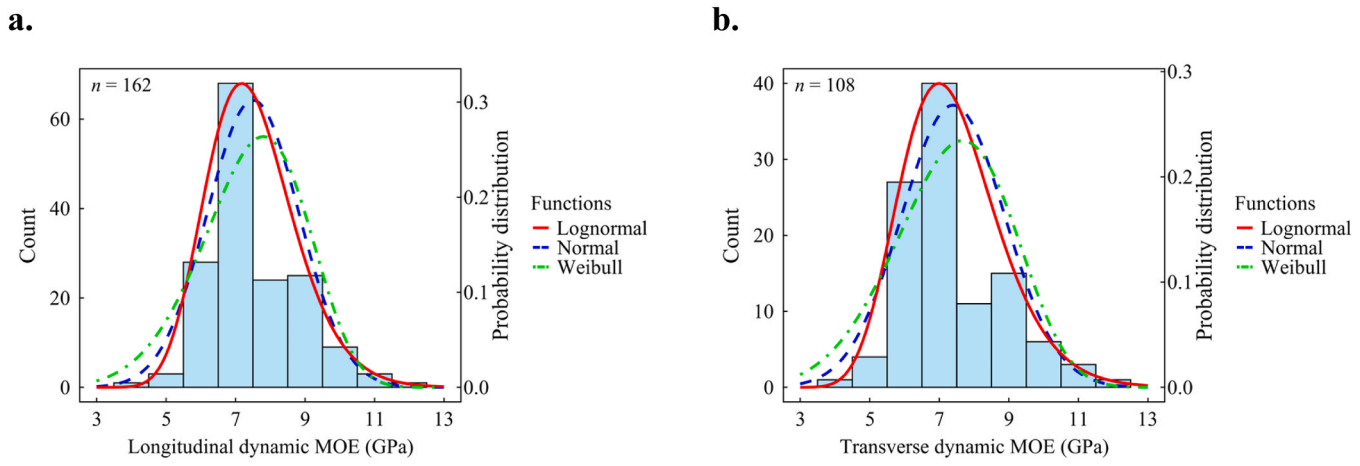

Fig. 5. Frequency histograms of (a) longitudinal and (b) transverse dynamic MOE with fitted probability distributions.

Table 3
Goodness-of-fit and model comparison based on one-sample K-S test and AIC for dynamic MOE.

Dynamic MOE	Hypothetical distribution	Parameters					Judgement	AIC
Longitudinal	Normal distribution	μ	σ	D_n	$D_{n,0.05}$	p-value		
		7.5023	1.3169	0.1225	0.1067	0.0155	refuse	552.93
	Lognormal distribution	2.0004	0.1713	0.0879	0.1067	0.1634	accept	540.21
	Weibull distribution	k	λ	D_n	$D_{n,0.05}$	p-value		
		5.6914	8.0679	0.1388	0.1067	0.0039	refuse	574.09
Transverse	Normal distribution	μ	σ	D_n	$D_{n,0.05}$	p-value		
		7.3987	1.4809	0.1487	0.1307	0.0169	refuse	395.31
	Lognormal distribution	1.9822	0.1939	0.1091	0.1307	0.1530	accept	384.32
	Weibull distribution	k	λ	D_n	$D_{n,0.05}$	p-value		
		5.0006	8.0168	0.1631	0.1307	0.0064	refuse	407.79

Table 4
Sample statistics and fitted lognormal distribution parameters for dynamic MOE.

Dynamic MOE	Sample statistics			Fitted lognormal distribution statistics			
	Mean	Sd	Cv	$E(X)$	$\sigma(X)$	$P_{5,75}$	$P_{95,75}$
Longitudinal	7.5023	1.3210	17.6079	7.5017	1.2986	5.4481	10.0291
Transverse	7.3987	1.4878	20.1095	7.3979	1.4549	5.1267	10.2778

Note: $P_{5,75}$ and $P_{95,75}$ represent the 5th percentile and 95th percentile values, respectively, at a 75 % confidence level for the corresponding distributions.

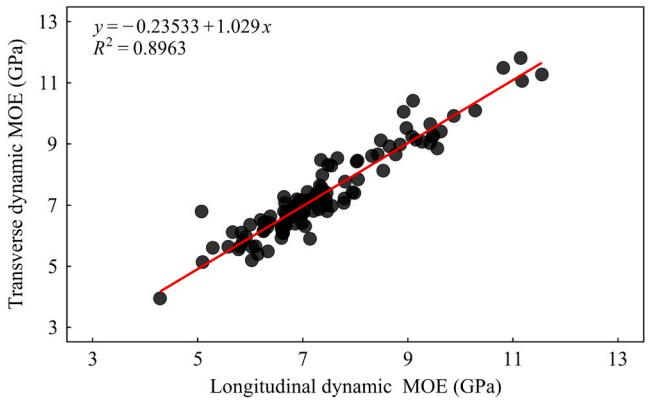

Fig. 6. Regression relationship between longitudinal and transverse dynamic MOE.

the material properties and resonance frequency.

As established in the preceding sections, the lognormal distribution is identified as the optimal model for both the global density and the longitudinal dynamic MOE. Their corresponding probability density functions are expressed as:

$$f_{E_{\mathrm{dyn,l,12}}}\left(x;\mu_{E_{\mathrm{dyn,l,12}}},\sigma_{E_{\mathrm{dyn,l,12}}}\right)=\frac{1}{x\sigma_{E_{\mathrm{dyn,l,12}}}\sqrt{2\pi}}e^{-\left(\ln x-\mu_{E_{\mathrm{dyn,l,12}}}\right)^2\Big/2\sigma_{E_{\mathrm{dyn,l,12}}}{}^2} \tag{29}$$

Where $\mu_{E_{\mathrm{dyn,l,12}}}=2.0004$ and $\sigma_{E_{\mathrm{dyn,l,12}}}=0.1713$ (Table 3).

$$f_{\rho_{12}}\left(x;\mu_{\rho_{12}},\sigma_{\rho_{12}}\right)=\frac{1}{x\sigma_{\rho_{12}}\sqrt{2\pi}}e^{-\left(\ln x-\mu_{\rho_{12}}\right)^2/2\sigma_{\rho_{12}}{}^2} \tag{30}$$

Where $\mu_{\rho_{12}}=5.8428$ and $\sigma_{\rho_{12}}=0.1218$ (Table 2).

Using these probabilistic models, a Monte Carlo simulation was performed to predict the theoretical distribution of resonance frequencies [31]. For each specimen length, N random pairs of $E_{\mathrm{dyn,l,12}}$ and ρ_{12} were generated. The first longitudinal resonance frequency for each pair (i) was then calculated using Eq. (31):

$$f^{(i)}=\sqrt{\frac{{E_{\mathrm{dyn,l,12}}}^{(i)}}{4.062728\times10^{-9}\bullet{\rho_{12}}^{(i)}L^2}} \tag{31}$$

A convergence analysis was conducted to determine the optimal number of Monte Carlo simulations and ensure the stability of the results. The number of random samples (N) was varied from 500 to 100000 in increments of 500. For each N, the simulation was repeated 20 runs, and in each run, the mean value of the simulated resonance frequencies was taken as the predicted value. Two relative error metrics

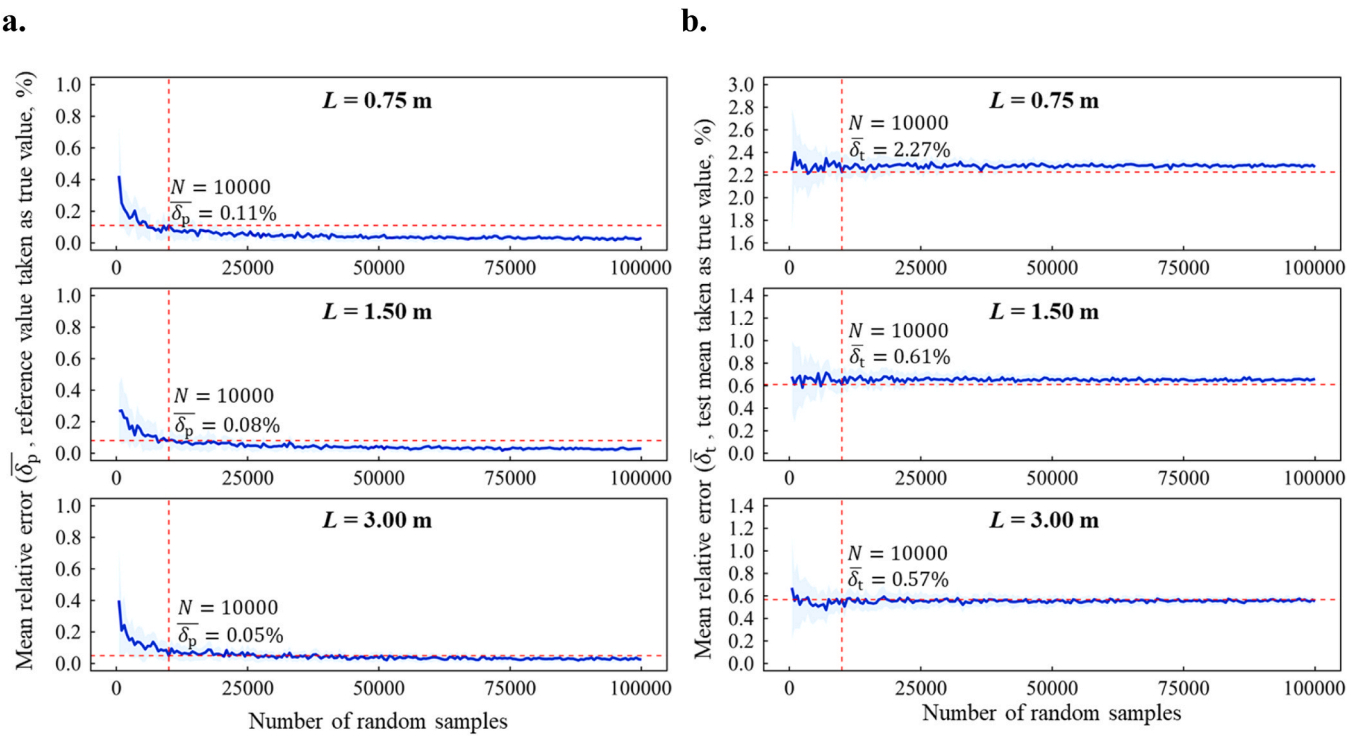

Fig. 7. Convergence analysis of Monte Carlo simulations. The blue solid line represents the mean relative error calculated from 20 independent runs for each sample size (N), and the shaded ribbon indicates the standard deviation of the error across these runs. In (a), the reference value corresponds to the mean frequency predicted at N = 1000000.

were defined: δ_p, representing the relative error when the mean frequency predicted at $N = 1000000$ (reference value) is taken as the true value, and δ_t, representing the relative error when the experimentally measured mean frequency is taken as the true value.

As shown in Fig. 7-a, the mean of δ_p ($\overline{\delta_p}$) decreases as N increases. While a slight decrease in δ_p is observed beyond $N = 10000$, the maximum error across all specimen dimensions is merely 0.11 % at this point, which is negligible for practical purposes. Meanwhile, the mean of δ_t ($\overline{\delta_t}$) also stabilizes around $N = 10000$, although its standard deviation continues to decrease slowly with larger N (Fig. 7-b). These results demonstrate that the estimates converge and become highly stable at $N = 10000$. Therefore, a single run with $N = 10000$ is considered sufficient for reliable frequency estimation and is adopted in all subsequent analyses.

Fig. 8-a illustrates the decreasing trend of the first longitudinal resonance frequency as the specimen length increases, while Fig. 8-b presents the probability distribution of the resonance frequency for specimens with a length of 3 m. Table 5 provides a summary of both the statistical results from the experiments and the corresponding theoretical predictions across different specimen lengths.

The resonance frequency declines from 3081.03 Hz at 0.75 m to 770.26 Hz at 3 m. Additionally, the 95 % confidence intervals become narrower with increasing length—from [2490.41–3757.27 Hz] at 0.75 m to [622.60–939.32 Hz] at 3 m—indicating reduced variability in longer specimens. The theoretical mean frequencies show strong agreement with the experimental means; for instance, at 1.5 m, the theoretical value is 1540.52 Hz, closely matching the sample mean of 1550.16 Hz. Furthermore, the observed frequency range falls within the predicted confidence intervals, and the maximum absolute mean prediction error is 2.31 %, supporting the reliability of the theoretical model in estimating resonance frequencies across various specimen lengths.

3.1.3.2. Transverse resonance frequency. Similar to the longitudinal case, predicting the transverse resonance frequency requires incorporating both the transverse dynamic MOE and global density distributions, combined with a Monte Carlo simulation.

However, Eq. (4) does not explicitly include the density term, so it must be transformed accordingly. Substituting $m = \rho V = \rho AL$ and $I = A \bullet i^2$, where ρ denotes ρ_{global} of Eq. (2), A is the area of cross-section, i is the radius of gyration, Eq. (4) becomes:

$$E_{dyn,t,12} = \left(\frac{2f_1}{\gamma_1 \bullet \pi}\right)^2 \bullet \frac{\rho L^4}{i^2} = \frac{(2\pi f_1)^2}{(\sqrt{\gamma_1} \bullet \pi)^4} \bullet \frac{\rho L^4}{i^2}\left(1 + \frac{u_s - 12}{100}\right) \times 10^{-9} \tag{32}$$

Using Eq. (32), a size-related dimension factor $D = \frac{L^4}{i^2} = \frac{12L^4}{h^2}$ is introduced. Combining this with Eq. (2) and incorporating moisture correction, the transverse dynamic MOE at 12 % moisture content is expressed as Eq. (33), where ρ_{12} also denotes $\rho_{global,12}$ from Eq. (2):

$$E_{dyn,t,12} = D \bullet \rho_{12} \bullet \frac{(2\pi f_1)^2}{(\sqrt{\gamma_1} \bullet \pi)^4} \bullet \left(\frac{1 + 0.01(u_s - 12)}{1 - 0.005(u_s - 12)}\right) \times 10^{-9} \tag{33}$$

Given that the average moisture content was 13.04 %, substituting $u_s = 13.04$ and $\gamma_1 = 2.267$ into Eq. (33) simplifies it to Eq. (34):

$$f_1 = \sqrt{\frac{E_{dyn,t,12}}{8.010742 \times 10^{-11} \bullet \rho_{12} D}} \tag{34}$$

The transverse dynamic MOE follows a lognormal probability distribution, and the corresponding probability density function is given by Eq. (35), while that of ρ_{12} is defined by Eq. (30) before.

$$f_{E_{dyn,t,12}}\left(x; \mu_{E_{dyn,t,12}}, \sigma_{E_{dyn,t,12}}\right) = \frac{1}{x\sigma_{E_{dyn,t,12}}\sqrt{2\pi}} e^{-\left(\ln x - \mu_{E_{dyn,t,12}}\right)^2 \Big/ 2\sigma_{E_{dyn,t,12}}^2} \tag{35}$$

Where $\mu_{E_{dyn,t,12}} = 1.9822$ and $\sigma_{E_{dyn,t,12}} = 0.1939$ (Table 3).

Monte Carlo simulation was subsequently employed to compute the resonance frequency distribution:

$$f_1^{(i)} = \sqrt{\frac{E_{dyn,t,12}^{(i)}}{8.010742 \times 10^{-11} \bullet \rho_{12}^{(i)} D}} \tag{36}$$

The convergence analysis of transverse resonance frequency simulations yielded results consistent with those obtained for longitudinal resonance frequencies. Therefore, only the case with $N = 10000$ samples was analyzed in this section.

Table 6 summarizes theoretical and sample statistics of first transverse resonance frequencies for varying lengths and thicknesses. Theoretical means decrease with increasing length and increase with increasing thickness. For example, at 13 mm thickness, theoretical mean drops from 108.96 Hz (0.75 m) to 6.81 Hz (3.0 m). At fixed length (0.75 m), increasing thickness raises the mean from 108.96 Hz (13 mm) to 292.59 Hz (35 mm). The sample test means are in close agreement with the theoretical predictions, with a maximum absolute mean prediction error is 4.52 %. Furthermore, the observed min–max values generally fall within theoretical confidence intervals.

Notably, for the 3 m specimens, the mean transverse resonance frequency predicted by the simulation fell below the lower detection limit of the testing equipment, which is consistent with the experimental observation that these specimens could not be successfully measured.

These findings indicate the potential of estimating resonance

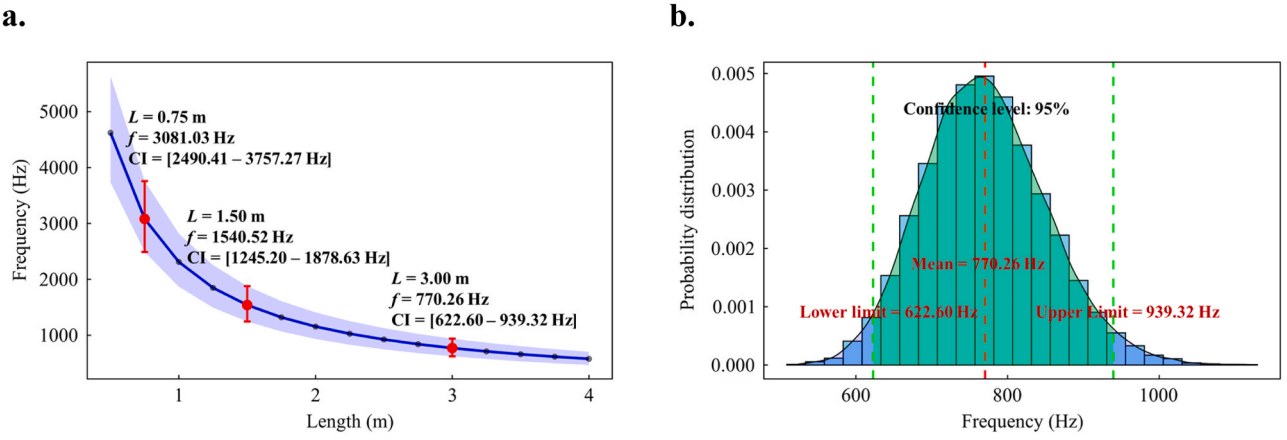

Fig. 8. Theoretical prediction of the first longitudinal resonance frequency: (a) Variation of the first longitudinal resonance frequency with length; (b) An example with a length of 3 m.

Table 5
Statistical summary of the first longitudinal resonance frequency of specimens: comparison between test measurements and theoretical calculations.

Length (m)	Theoretical calculation (Hz)				Test (Hz)				Absolute error of mean (%)
	Mean	Sd	Lower CI	Upper CI	Mean	Sd	Min	Max	
0.75	3081.03	323.14	2490.41	3757.27	3011.33	239.56	2377.07	3541.35	2.31
1.50	1540.52	161.57	1245.20	1878.63	1550.16	135.65	1283.23	1865.74	0.62
3.00	770.26	80.79	622.60	939.32	774.33	62.92	614.71	889.91	0.53

Table 6
Statistical summary of sampled and theoretically calculated first transverse resonance frequencies.

Length (m)	Thickness (mm)	Theoretical prediction (Hz)				Test (Hz)				Absolute error of mean (%)
		Mean	Sd	Lower CI	Upper CI	Mean	Sd	Min	Max	
0.75	13	108.96	12.52	86.34	135.29	110.15	16.45	90.72	146.92	1.08
0.75	18	151.00	17.44	119.48	187.91	144.47	11.93	128.63	167.45	4.52
0.75	35	292.59	33.85	232.52	363.55	296.22	21.65	236.53	327.84	1.23
1.50	13	27.21	3.15	21.57	33.86	26.05	2.82	21.46	32.22	4.45
1.50	18	37.75	4.32	30.10	47.16	39.01	2.90	33.82	44.35	3.23
1.50	35	73.17	8.40	58.31	90.80	75.15	4.13	69.56	84.76	2.63
3.00	13	6.81	0.78	5.39	8.44					
3.00	18	9.42	1.07	7.46	11.70					
3.00	35	18.32	2.14	14.51	22.86					

frequencies using randomly selected specimens characterized by nominal dimensions, dynamic MOEs, and densities. This method is well suited for field testing scenarios, as setting appropriate resonance frequency intervals can help reduce the influence of external noise and resonance interference.

3.2. Static bending tests

Fig. 9 illustrates the frequency histograms of bending MOE and bending strength, overlaid with fitted curves for normal, lognormal, and Weibull distributions. Table 7 reports the results of goodness-of-fit and model comparison based on one-sample K–S test and AIC.

For the bending MOE, both normal and lognormal distributions are acceptable. The normal fit yields AIC = 563.85, and the lognormal fit performs better, with AIC = 548.27, indicating superior agreement. Bending strength data also conform to all three distributions. Among these, the lognormal distribution shows the smallest value of AIC (1284.62), indicating a relatively better fit.

Table 8 presents the sample mean, standard deviation, coefficient of variation, and the expected value and standard deviation under the lognormal distribution, as well as the 5th and 95th percentile values at a 75 % confidence level for both bending MOE and bending strength [30]. The expected value of the fitted lognormal for bending MOE is 5.7716 GPa, identical to the sample mean. For bending strength, the lognormal expectation is 44.6567 MPa, closely matching the sample mean of 44.4967 MPa.

3.3. Regression models for lamina grading

Fig. 10 presents the regression between global density and bending properties. The coefficient of determination is low for both bending MOE (R^2 = 0.1826) and strength (R^2 = 0.1789), indicating weak correlations. Figs. 11 and 12 show regressions of longitudinal and transverse dynamic MOE against bending properties. Transverse dynamic MOE demonstrates slightly better predictive performance, with R^2 = 0.3717 for bending MOE and R^2 = 0.4498 for bending strength, compared with R^2 = 0.3548 and R^2 = 0.4043, respectively, for the longitudinal dynamic MOE.

These R^2 values are lower than those reported in previous studies [13,32], mainly due to: (1) The use of flatwise three-point bending with short spans, leading to more localized variability, while dynamic MOE reflects global stiffness; (2) The inherently higher variability in mechanical properties of fast-grown Chinese fir; (3) The inclusion of mixed-dimension specimens, introducing size effects that weaken correlations compared with uniform-size datasets.

Despite these limitations, subsequent grading results demonstrate

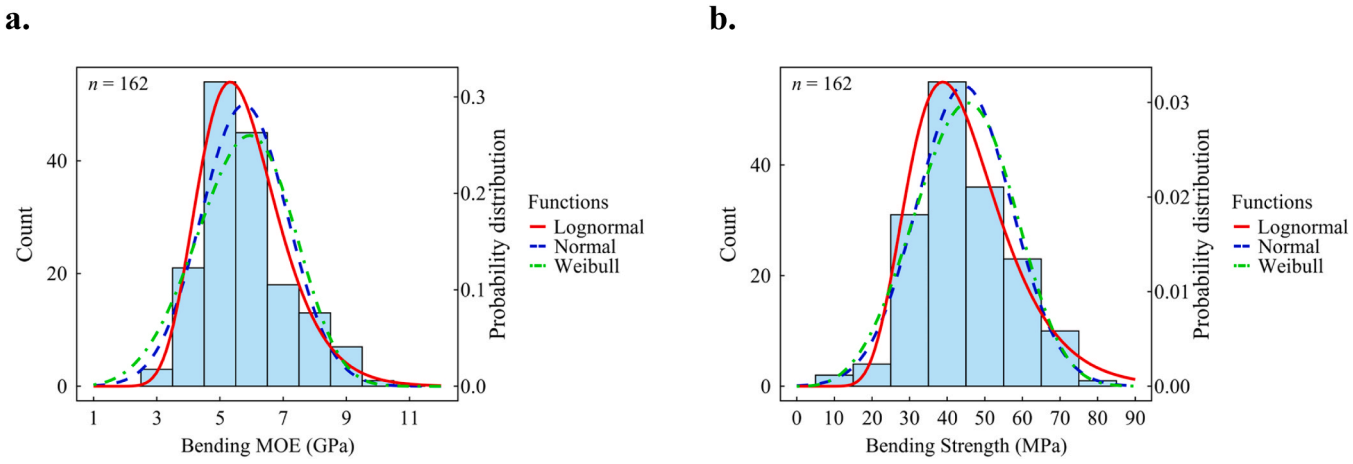

Fig. 9. Frequency histograms and fitted probability distributions of (a) bending MOE and (b) bending strength.

Table 7
Goodness-of-fit and model comparison based on one-sample K-S test and AIC for bending MOE and bending strength.

Bending property	Hypothetical distribution	Parameters					Judgement	AIC
E	Normal distribution	μ	σ	D_n	$D_{n,0.05}$	p-value		
		5.7716	1.3621	0.1049	0.1067	0.0567	accept	563.85
	Lognormal distribution	1.7261	0.2310	0.0592	0.1067	0.6223	accept	548.27
	Weibull distribution	k	λ	D_n	$D_{n,0.05}$	p-value		
		4.3369	6.3147	0.1191	0.1067	0.0201	refuse	575.99
f	Normal distribution	μ	σ	D_n	$D_{n,0.05}$	p-value		
		44.4967	12.5296	0.0786	0.1067	0.2693	accept	1292.84
	Lognormal distribution	3.7522	0.3049	0.0633	0.1067	0.5344	accept	1284.62
	Weibull distribution	k	λ	D_n	$D_{n,0.05}$	p-value		
		3.8557	49.1556	0.0808	0.1067	0.2405	accept	1294.81

Table 8
Sample statistics and fitted lognormal distribution parameters for bending MOE and bending strength.

Bending property	Sample statistics			Fitted lognormal distribution statistics			
	Mean	Sd	Cv	$E(X)$	$\sigma(X)$	$P_{5,75}$	$P_{95,75}$
E	5.7716	1.3663	23.67	5.7716	1.3557	3.7233	8.4791
f	44.4967	12.5684	28.2458	44.6567	13.9837	24.7583	73.3546

Note: $P_{5,75}$ and $P_{95,75}$ represent the 5th percentile and 95th percentile values, respectively, at a 75 % confidence level for the corresponding distributions.

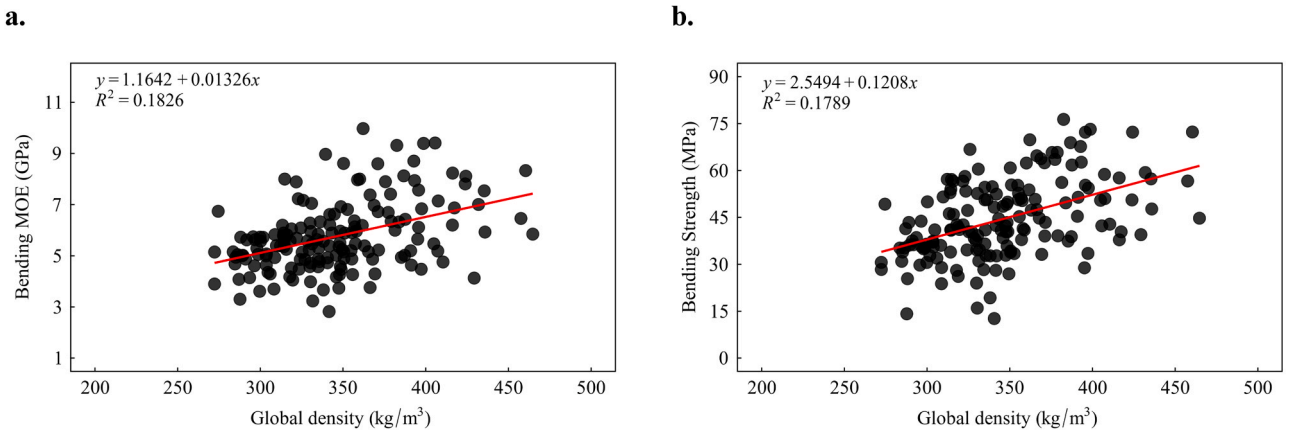

Fig. 10. Regression relationships between global density and (a) bending MOE and (b) bending strength.

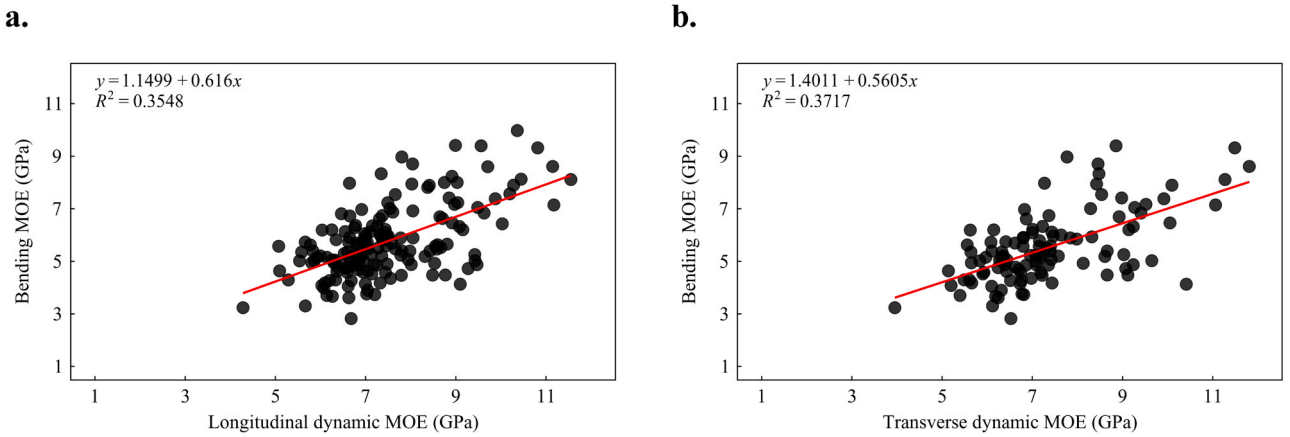

Fig. 11. Regression relationships between dynamic MOE and bending MOE: (a) longitudinal dynamic MOE vs. bending MOE; (b) transverse dynamic MOE vs. bending MOE.

that mixed-size laminae can still effectively differentiate bending properties among grades.

3.4. Lamina grading results

In factory production, timber is commonly graded using the longitudinal dynamic MOE [14]. Accordingly, the grading model in this study

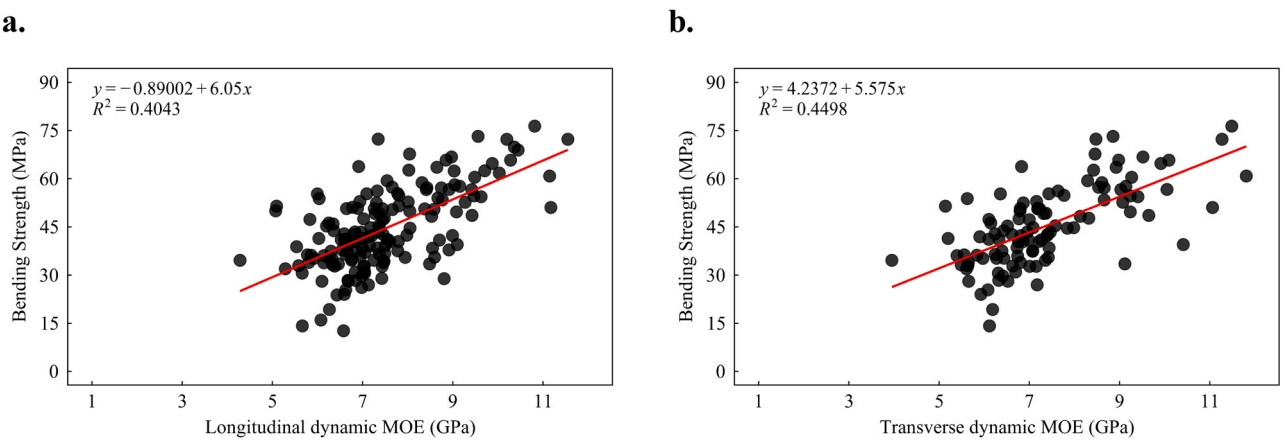

Fig. 12. Regression relationships between dynamic MOE and bending strength from four-point bending tests: (a) longitudinal dynamic MOE vs. bending strength; (b) transverse dynamic MOE vs. bending strength.

is developed based solely on longitudinal dynamic MOE. Model parameters derived from regression results are listed in Table 9. Target dynamic MOE values for each grade are calculated using Eq. (12) – Eq. (17) (results in Table 10), and a summary of specimen statistics after grading is provided in Table 11.

Results show that specimens are classified into six grades: L30, L40, L50, L60, L70, and Reject. L40 includes the most specimens (77, 47.5 %), while L70 and the reject group each have only 4 (2.5 %).

To assess whether the graded specimens meet bending property requirements, regression lines between bending MOE and bending strength were established, along with a 95 % prediction lower limit. The resulting lower limit ($f_{0.05}$) is calculated as:

$$f_{0.05} = b_f + a_f E - t_{\alpha,n-2}\sqrt{\frac{{s_{\delta f}}^2}{n}\left[1 + \frac{(E-\overline{E})^2}{{s_E}^2}\right] + {s_{\delta f}}^2} \quad (37)$$

Where $f_{0.05}$ represents the 95 % prediction lower limit of the bending strength corresponding to a given E, b_f and a_f are the estimated intercept and slope of the regression equation between f and E ($b_f = 10.207$, $a_f = 5.94$), α is the significance level (here $\alpha = 0.05$), n is the sample size ($n = 162$), s_E is the standard deviation of bending MOE, $t_{\alpha,n-2} = t_{0.05,160} = 1.654$, $s_{\delta f}$ is the residual standard deviation of the regression equation established between f and E.

Using the intercept derived from the regression model established between $f_{0.05}$ and the corresponding values of E, the following relationship is obtained and expressed in Eq. (38):

$$f_{0.05} = -5.6655 + 5.94E \quad (38)$$

Fig. 13 displays these regression lines, showing that both the predicted strength and its lower limit exceed the grade requirements, supporting the reliability of the grading. Fig. 14 further presents the lognormal distribution of bending properties per grade. Mean values for MOE and strength meet standard thresholds. However, For L60, the 5th percentile of MOE at 75 % confidence is 4.2 GPa, below the 5.0 GPa standard; for L70, the 5th percentile of strength is 39.3 MPa, lower than that of L60 (47.6 MPa). These results indicate that larger sample sizes or a stricter prediction lower limit are needed to improve grading robustness in future.

Table 9
Regression models for bending MOE and bending strength and statistical parameters required for grading setting calculations.

Model	R^2	a	b	s_δ	t
$E = 1.1499 + 0.616E_{dyn,l,12}$	0.3548	0.616	1.1499	1.1009	1.645
$f = -0.89002 + 6.05E_{dyn,l,12}$	0.4043	6.05	-0.8900	9.7308	1.645

Table 10
Calculated dynamic MOE setting values for strength classes in JAS 1152 [21].

Grade	Setting (GPa)					Range of $E_{dyn,l,12}$
	$S_{E,mean}$	$S_{E,05}$	$S_{f,mean}$	$S_{f,05}$	S	
Reject						< 5.4
L30	3.0	5.1	3.6	5.4	5.4	≥ 5.4 and < 6.4
L40	4.6	6.4	4.1	5.8	6.4	≥ 6.4 and < 7.7
L50	6.2	7.7	4.6	6.2	7.7	≥ 7.7 and < 9.2
L60	7.9	9.2	5.1	6.5	9.2	≥ 9.2 and < 10.8
L70	9.5	10.8	5.6	6.9	10.8	≥ 10.8 and < 11.6
L80	11.1	11.6	6.1	7.3	11.6	≥ 11.6 and < S of L90

Note: Settings for other strength classes can also be calculated using Eq. (12) – Eq. (17), which are not listed here.

As shown in Table 10 and Table 11, the bending MOE, particularly its lower limit, serves as the primary constraint in strength grading. In contrast, the bending strength within each grade consistently exceeds the required thresholds—for instance, L60 specimens exhibit a mean strength of 61.9 MPa and a 5th percentile value (75 % confidence) of 47.8 MPa, satisfying the L140 (mean 54 MPa, lower limit 40.5 MPa) and approaching the L160 (mean 63 MPa, lower limit 47.5 MPa). Under the current testing conditions, this indicates that for Chinese fir, bending strength testing may not be necessary during the derivation of grading thresholds—dynamic MOE values alone can be calibrated based on static bending MOE to define strength classes.

Future research will aim to validate this excess strength in Chinese fir strength grading and may inform revisions to relevant standards to better capitalize on the material's relatively high bending strength. In addition, further investigations will assess the influence of grading based on single-size groups versus mixed-size specimens, as well as evaluate the impact of the edgewise bending test (as adopted in EN 338 [33]) on the predictive accuracy of regression-based grading models for Chinese fir.

4. Conclusion

This study focused on fast-grown Chinese fir timber, designing laminae of various dimensions and measuring dynamic MOE using resonance frequency methods. Based on static bending tests, grading models were established and grading thresholds were derived. The main conclusions are as follows:

1. Goodness-of-fit and model comparison, evaluated through the one-sample K-S test and AIC, demonstrate that the lognormal distribution provides a superior fit for the density, dynamic MOE, bending MOE, and bending strength.

Table 11
Statistics of specimens of assigned grades.

Grade	Strength class specification in JAS 1152 [21]				Assigned grade				Number	Ratio (%)
	E (GPa)		*f* (MPa)		*E* (GPa)		*f* (MPa)			
	Mean	Lower limit	Mean	Lower limit	Mean	$P_{5,75}$	Mean	$P_{5,75}$		
Reject					4.4	2.4	42.0	21.1	4	2.5
L30	3.0	2.5	21.0	16.0	4.9	3.5	36.3	18.8	26	16.0
L40	4.0	3.3	24.0	18.0	5.5	3.8	40.4	24.4	77	47.5
L50	5.0	4.1	27.0	20.5	6.3	4.1	50.3	32.9	37	22.8
L60	6.0	5.0	30.0	22.5	7.1	4.2	61.9	47.8	14	8.6
L70	7.0	6.0	33.0	25.0	8.3	6.1	65.1	39.3	4	2.5
L80	8.0	6.5	36.0	27.0					0	0.0
Total									162	100

Note: $P_{5,75}$ represent the 5th percentile at a 75 % confidence level.

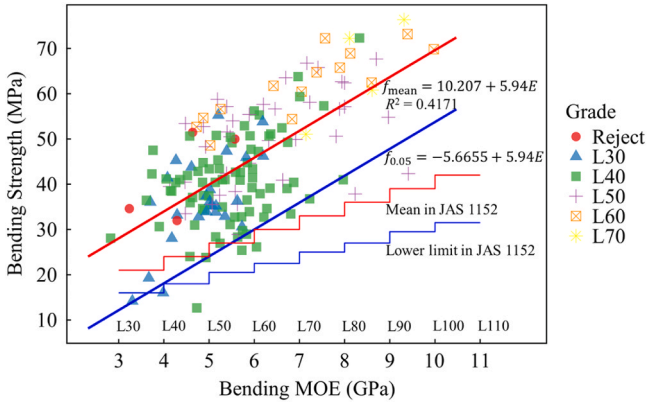

Fig. 13. Regression lines and their 95 % prediction lower limits for bending MOE and bending strength across assigned grades.Note: The vertical lines represent the 5th percentile values at a 75 % confidence level, as listed in Table 11.

2. Monte Carlo simulations are used to obtain theoretical calculations of the first longitudinal and transverse resonance frequencies relative to specimen dimension. The simulated mean values closely match theoretical calculations, with the maximum absolute errors for longitudinal and transverse frequencies being 2.31 % and 4.52 %. This provides a reliable reference for rapid and accurate measurement of first resonance frequencies in specimens of different dimensions.
3. Based on regression models correlating longitudinal dynamic MOE with bending MOE and bending strength, threshold values of dynamic MOE corresponding to JAS 1152 grading classes are derived. Samples are classified into six grades (including reject grade), with L40 containing the largest number of samples (77 pieces, accounting for 47.5 %). The mean and lower limit of bending MOE and bending strength of each grade meet the standard requirements, except the 5th percentile (at 75 % confidence level) of bending MOE for the L60 grade (4.2 GPa) was below the standard lower limit (5.0 GPa).
4. The bending MOE, especially its lower limit, is the key mechanical property that determines the grading. An excess in bending strength exists across grades. For example, the L60 grade samples show an average bending strength of 61.9 MPa and a 5th percentile value (75 % confidence) of 47.8 MPa, which satisfies the requirements for the L140 grade in the standard (mean 54 MPa, lower limit 40.5 MPa) and approaches the L160 grade requirements (mean 63 MPa, lower limit 47.5 MPa). This indicates that for Chinese fir, bending strength testing may not be necessary during the derivation of grading thresholds.

CRediT authorship contribution statement

Jianzhang Li: Resources. **Shuke Jia:** Writing – review & editing. **Zeli Que:** Supervision, Project administration, Funding acquisition. **Fanxu Kong:** Writing – original draft, Methodology, Formal analysis, Data curation, Conceptualization. **Jingkang Lin:** Writing – review & editing, Validation, Resources. **Baolei Jin:** Writing – review & editing, Investigation. **Chenyang Jin:** Writing – review & editing. **Yihe Ni:** Investigation, Data curation. **Jiangbo Du:** Writing – review & editing, Resources.

Declaration of Competing Interest

The authors declare that they have no known competing financial

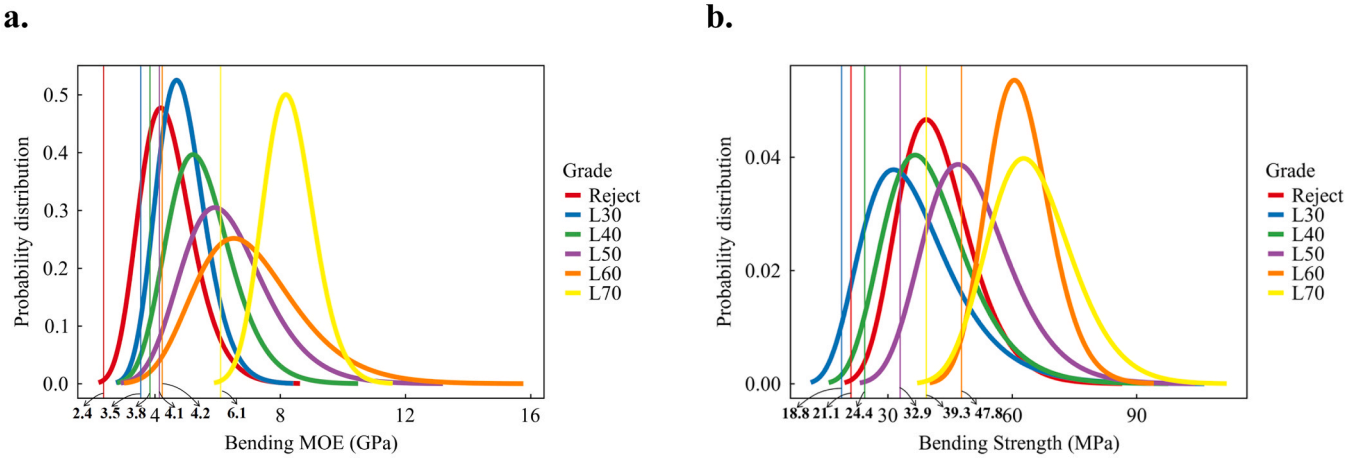

Fig. 14. Lognormal probability distributions of (a) bending MOE and (b) bending strength across assigned grades.

interests or personal relationships that could have appeared to influence the work reported in this paper.

Acknowledgments

The authors gratefully acknowledge the financial support provided by the National Key Research and Development Program of China (Grant No. 2024YFD2201204) and the Postgraduate Research & Practice Innovation Program of Jiangsu Province (Grant No. KYCX25–1415).

Data availability

Data will be made available on request.

References

[1] H. Li, B.J. Wang, P. Wei, L. Wang, Cross-laminated Timber (CLT) in China: a state-of-the-art, J. Bioresour. Bioprod. 4 (2019) 22–30, https://doi.org/10.21967/jbb.v4i1.190.
[2] I. Lukacs, A. Björnfot, R. Tomasi, Strength and stiffness of cross-laminated timber (CLT) shear walls: state-of-the-art of analytical approaches, Eng. Struct. 178 (2019) 136–147, https://doi.org/10.1016/j.engstruct.2018.05.126.
[3] J. Ou, Z. Chen, W. Long, D. Chen, L. Huo, Y. Zhang, Research on stability of CLT wall under uniform compression based on orthotropic plate buckling theory, J. Build. Eng. 84 (2024) 108571, https://doi.org/10.1016/j.jobe.2024.108571.
[4] Y. Wang, X. Sun, C. Zhu, China's wood-based forest product imports and exports: trends and implications, Int. For. Rev. 25 (2023) 503–516, https://doi.org/10.1505/146554823838028184.
[5] H.E. Ilgın, M. Karjalainen, P. Mikkola, Views of Cross-laminated timber (CLT) manufacturer representatives around the world on CLT Practices and its future outlook, Buildings 13 (2023) 2912, https://doi.org/10.3390/buildings13122912.
[6] Y. Gong, X. Chen, H. Ren, B. Liu, H. Zhang, Y. Wang, Theoretical and experimental studies on the bending properties of glued laminated timber manufactured with Chinese fir, Structures 68 (2024) 107149, https://doi.org/10.1016/j.istruc.2024.107149.
[7] National Forestry and Grassland Administration. China Forest Resource Report (2014-2018). China Forestry Publishing House, Beijing, China, 2019.
[8] F. Kong, B. Zhou, X. An, F. Wang, S. Wang, P. Ma, Z. Que, Experimental investigation on mechanical properties of Chinese fir composites as cross-laminated timber, Ind. Crops Prod. 213 (2024) 118411, https://doi.org/10.1016/j.indcrop.2024.118411.
[9] C. Tao, M. Li, K. Lin, X. Ma, J. Lin, P. Wu, Comparison of wood assortment structures among different clone Chinese fir plantations (in Chinese), J. For. Environ. 41 (2021) 204.
[10] P. Ma, X. An, F. Wang, H. Huang, Z. Chen, S. Wang, M. Gong, Z. Que, Effects of pre-heating treatment parameters on dimensional stability and mechanical properties of densified Chinese fir, Constr. Build. Mater. 407 (2023) 133484, https://doi.org/10.1016/j.conbuildmat.2023.133484.
[11] Z. Que, Z. Li, X. Zhang, Z. Yuan, B. Pan, Traditional Wooden Buildings in China. Wood in Civil Engineering, InTech, 2017, https://doi.org/10.5772/66145.
[12] F. Arriaga, J. Monton, E. Segues, G. Íñiguez-Gonzalez, Determination of the mechanical properties of radiata pine timber by means of longitudinal and transverse vibration methods, Holzforschung 68 (2014) 299–305, https://doi.org/10.1515/hf-2013-0087.
[13] A. Kovryga, J.O. Chuquin Gamarra, J.W.G. Van De Kuilen, Strength and stiffness predictions with focus on different acoustic measurement methods, Eur. J. Wood Wood Prod. 78 (2020) 941–949, https://doi.org/10.1007/s00107-020-01584-z.
[14] A. Olsson, J. Oscarsson, Strength grading on the basis of high resolution laser scanning and dynamic excitation: a full scale investigation of performance, Eur. J. Wood Wood Prod. 75 (2017) 17–31, https://doi.org/10.1007/s00107-016-1102-6.
[15] F.J.N. Franca, R.D. Seale, R. Shmulsky, T.S.F.A. Franca, Assessing southern pine 2×4 and 2×6 lumber quality: longitudinal and transverse vibration, Wood Fiber Sci. 51 (2019) 2–15, https://doi.org/10.22382/wfs-2019-002.
[16] A. Ettelaei, A. Taoum, G. Nolan, Assessment of different measurement methods/techniques in predicting modulus of elasticity of plantation Eucalyptus nitens timber for structural purposes, Forests 13 (2022) 607, https://doi.org/10.3390/f13040607.
[17] M. Balasso, M. Hunt, A. Jacobs, J. O'Reilly-Wapstra, Development of non-destructive-testing based selection and grading strategies for plantation Eucalyptus nitens sawn boards, Forests 12 (2021) 343, https://doi.org/10.3390/f12030343.
[18] J. Ou, Y. Zhang, W. Long, D. Chen, Y. Zhong, Bending properties of glulam made by domestic fast-growing Chinese fir (in Chinese), J. Build. Mater. 12 (2023) 1286, https: //doi:10.3969/j.issn.1007-9629.2023.12.007.
[19] Standardization Administration of China, Structural glued laminated timber. GB/T 26899–2022, Standards Press of China, Beijing, 2022.
[20] T. Yin, L. He, Q. Huang, Y. Gong, Z. Wang, M. Gong, Effect of lamination grade on bending and shear properties of CLT made from fast-growing Chinese fir, Ind. Crops Prod. 207 (2024) 117741, https://doi.org/10.1016/j.indcrop.2023.117741.
[21] Ministry of Agriculture, Forestry and Fisheries of Japan, Glued Laminated Timber. JAS 1152, Japanese Agricultural Standards Association, Tokyo, 2023.
[22] Ministry of Agriculture, Forestry and Fisheries of Japan, Sawn lumber.. JAS 1083,, Japanese Agricultural Standards Association, Tokyo, 2019.
[23] European Committee for Standardization. Timber structures - Strength graded structural timber with rectangular cross section - Part 2: Machine grading; additional requirements for type testing, EN 14081-2, Brussels, Belgium, 2018.
[24] J.R. Benjamin, C.A. Cornell, Probability, statistics, and decision for civil engineers, Dover Publications, New York: McGraw-Hill, 1970.
[25] G. Marsaglia, W.W. Tsang, J. Wang, Evaluating Kolmogorov's distribution, J. Stat. Softw. 8 (2003), https://doi.org/10.18637/jss.v008.i18.
[26] F.J. Massey, The Kolmogorov-Smirnov test for goodness of fit, J. Am. Stat. Assoc. 46 (1951) 68–78.
[27] A. Zeimbekakis, E.D. Schifano, J. Yan, On misuses of the Kolmogorov–Smirnov test for one-sample Goodness-of-Fit, Am. Stat. 78 (2024) 481–487, https://doi.org/10.1080/00031305.2024.2356095.
[28] H. Akaike, A new look at the statistical model identification, IEEE Trans. Autom. Control 19 (6) (1974) 716–723, https://doi.org/10.1109/TAC.1974.1100705.
[29] R. Core Team, R: A Language and Environment for Statistical Computing, R Foundation for Statistical Computing, Vienna, Austria, 2024. ⟨https://www.R-project.org⟩.
[30] European Committee for Standardization, Timber structures – Calculation and verification of characteristic values, EN 14358, Brussels, Belgium, 2016.
[31] S. Raychaudhuri, Introduction to Monte Carlo simulation, in: S.J. Mason, R.R. Hill, L. Mönch, O. Rose, T. Jefferson, J.W. Fowler (Eds.), Proc. 2008 Winter Simulation Conference, IEEE, Miami, FL, USA, 2008, pp. 91–100.
[32] A. Vega, A. Dieste, M. Guaita, J. Majada, V. Baño, Modelling of the mechanical properties of Castanea sativa Mill. structural timber by a combination of non-destructive variables and visual grading parameters, Eur. J. Wood Wood Prod. 70 (2012) 839–844, https://doi.org/10.1007/s00107-012-0626-7.
[33] European Committee for Standardization, Structural timber — Strength classes. EN 338, Brussels, Belgium, 2016.